arXiv:2007.07534v1 [nlin.PS] 15 Jul 2020

Influence of Stimulated Raman Scattering on Kerr domain walls and localized structures

P. Parra-Rivas[1,2], S. Coulibaly[3], M. G. Clerc[4], and M. Tlidi[5]
[1] *OPERA-photonics, Université libre de Bruxelles, 50 Avenue F. D. Roosevelt, CP 194/5, B-1050 Bruxelles, Belgium*
[2] *Laboratory of Dynamics in Biological Systems, KU Leuven Department of Cellular and Molecular Medicine, University of Leuven, B-3000 Leuven, Belgium*
[3] *Université de Lille, CNRS, UMR 8523-PhLAM-Physique des Lasers Atomes et Molécules, F-59000 Lille, France*
[4] *Departamento de Física and Millennium Institute for Research in Optics, Facultad de Ciencias Físicas y Matemáticas, Universidad de Chile, Casilla 487-3, Santiago, Chile*
[5] *Faculté des Sciences, Université Libre de Bruxelles (U.L.B), CP 231, Campus Plaine, B-1050 Bruxelles, Belgium*
(Dated: January 27, 2022)

We investigate the influence of the stimulated Raman scattering on the formation of bright and dark localized states in all-fiber resonators subject to a coherent optical injection, when operating in the normal dispersion regime. In the absence of the Raman effect, and far from any modulational instability, localized structures form due to the locking of domain walls connecting two coexisting continuous wave states, and undergo a particular bifurcation structure known as collapsed snaking. The stimulated Raman scattering breaks the reflection symmetry of the system, and modifies the dynamics, stability, and locking of domain walls. This modification leads to the formation of, not only dark, but also bright moving localized states, which otherwise are absent. We perform a detailed bifurcation analysis of these localized states, and classify their dynamics and stability as a function of the main parameters of the system.

I. INTRODUCTION

Dissipative localized structures (LSs), also known as *dissipative solitons*, are coherent states emerging in extended systems far from the thermodynamic equilibrium [1–5]. Dissipative LSs may appear in a large variety of pattern forming systems ranging from fluid mechanics and optics, to biology and plant ecology [3–10]. These robust states can behave like discrete objects in continuous systems, and can display a variety of different dynamics such as periodic oscillations, chaos, or excitability [4, 5]. LSs evolve on macroscopic spatial scales, and can be only maintained by permanent non-equilibrium constraints, not being related with the intrinsic inhomogeneities of the system. Furthermore, once the system parameters are fixed, they are unique, and hence different from the well known conservative solitons that appear as one-parameter families [3, 4]. The formation of LSs is usually related with the presence of bi-stability between different coexisting steady states, and therefore LSs can be seen as a portion of one of those states embedded on the other one [11].

Classic examples of dissipative systems where LSs may emerge are found in the field of nonlinear optics and laser physics [3–5]. In this context, LSs have been widely studied in externally driven diffractive nonlinear cavities with cubic (i.e., Kerr) nonlinearities [12–15]. In these type of cavities, two dimensional LSs, consisting in spots of light embedded on a homogeneous background, form in the transverse plane to the propagation direction, and are commonly known as *spatial cavity solitons*. Similar types of LSs have been shown in wave-guided dispersive Kerr cavities, where they correspond to one-dimensional *temporal cavity solitons* emerging along the propagation direction [16–20]. Temporal LSs have been considered as the basis for all-optical buffering [16], and in the last decade, for broadband frequency combs generation in microresonators [21–23]. In both, diffractive and dispersive Kerr cavities, LSs emerge from a double balance between Kerr nonlinearity and spatial coupling (e.g., diffraction and/or dispersion) on one hand, and energy gain and losses on the other hand [3].

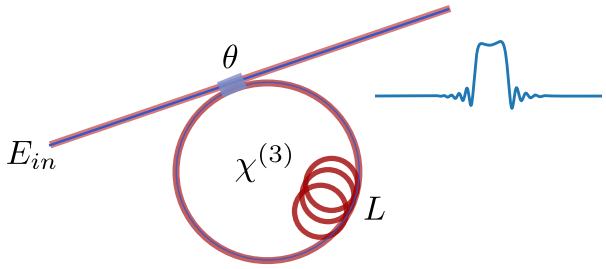


FIG. 1. Sketch of an all-fiber cavity of length L driven by an external laser beam of amplitude E_{in} through a beam splitter with intensity transmission coefficient θ. Dissipative structures of different type form and circulate along the cavity.

In dispersive Kerr cavities, temporal LSs can form in either the normal or anomalous dispersion regimes. In the normal regime, LSs arise due to the locking of domain walls (DWs), also known as switching waves or fronts, connecting two different continuous-wave (CW) states [19, 20, 24–26]. These LSs are different from those appearing in the anomalous regime, where their formation is related with the heteroclinic tangle of coexisting CW states and subcritical Turing patterns [16, 17, 27–29]. Close to the zero-dispersion wavelength, the influence of high-order effects, such as third and fourth-order dispersion, has to be considered. These terms may cause

important modifications on the LSs dynamics, such as the stabilization of different types of LSs, in both normal and anomalous regimes [30–35].

In systems made of amorphous materials, such as optical fibers, stimulated Raman scattering (SRS), originated from the delayed material response to electromagnetic excitation, may also have important implications on the LSs dynamics. These implications have been studied by many authors in the context of the anomalous dispersion regime, where most of the studies focus on the cavity soliton dynamics and stability [36–41].

In normal dispersion materials, the influence of SRS on the dynamics of DWs and LSs has also attracted an important attention in the last years [42–44]. In particular, it has been shown that SRS may stabilize moving bright LSs, which are absent otherwise [43]. Close to the nascent bistability onset, where the system can be described by a real order parameter equation, the DWs interaction and locking has been theoretically addressed, and an analytical expression for such interaction has been derived [43, 45]. However, as far as we known, a complete and detailed description of the bifurcation structure and stability of the LSs in this context is still lacking. Therefore, the aim of this article is to elucidate the implications that SRS may have, not only on the dynamics and stability of the different type of DWs and LSs arising in these systems, but also in their bifurcation structure.

The paper is organized as follows. In Section II, we introduce the model describing dispersive Kerr cavities in the presence of SRS. Section III focuses on the CW states and the formation of DWs. Later in Sec. IV, we introduce the mechanism of DWs locking for the formation of LSs, and we study their bifurcation structure in the absence of SRS. In Sec. V, we analyze the modification of the previous scenario when SRS is considered and how the SRS affects the formation of LSs. Sections VI and VII are devoted to the bifurcation and stability analysis of the Raman LSs. Here we classify the different dynamical regimes in terms of the main parameters of the system. Finally, in Sec. VIII, a short discussion and the main conclusions of our work are given.

II. THE LUGIATO-LEFEVER MODEL WITH STIMULATED RAMAN SCATTERING

We consider an all-fiber cavity of length L driven by a coherent injected field of amplitude E_{in} as shown in Fig. 1, where θ represents the intensity transmission coefficient of the beam splitter. The transmitted part of the injected field circulating within the cavity is affected by Kerr nonlinearity, chromatic dispersion, forcing, and dissipation. In the high-finesse limit, and in the presence of SRS, the intracavity field envelope E of the electric field

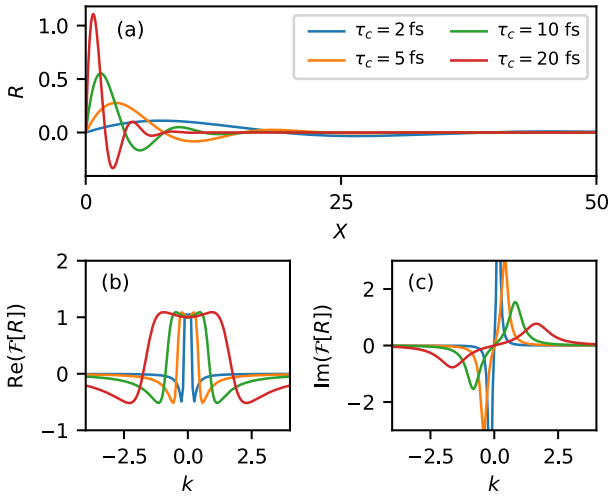


FIG. 2. In (a) the kernel associated with the SRS response function R for different values of the characteristic parameter τ_c. Panel (b) and (c) shows the real and imaginary parts of $\mathcal{F}[\mathsf{R}]$. Here $(\tau_1, \tau_2, f_R) = (12.2\text{ fs}, 32\text{ fs}, 0.18)$

is described by the extended Lugiato-Lefever equation

$$t_R\partial_t E = -(\alpha + i\delta_0)E + \sqrt{\theta}E_{in} - i\frac{\beta_2 L}{2}\partial_\tau^2 E + i\gamma L(1-f_R)|E|^2E + if_R L\gamma E\int_0^\infty R(\tau')|E(\tau-\tau')|^2 d\tau', \tag{1}$$

where τ is the fast time and t is the slow time, t_R is the round-trip time, γ is the nonlinear coefficient, β_2 is the chromatic dispersion coefficient, δ_0 is the phase detuning between the pump field and the nearest cavity resonance, and α represents the linear cavity losses [37, 46, 47]. The nonlocal delay response term models the SRS, and in agreement with experimental measurements, its kernel or influence function takes the form [48]

$$R(\tau) = \frac{\tau_1^2+\tau_2^2}{\tau_1\tau_2^2}e^{-\tau/\tau_2}\sin(\tau/\tau_1), \tag{2}$$

where the parameter f_R denotes the strength of the SRS term, and the parameters $\tau_{1,2}$ depend on the type of fiber. Note that in real systems, perturbations due to the higher order dispersion effects may be present alongside the SRS. However, in this theoretical study, for simplicity, we neglect those effects, and focus on the SRS.

The LL equation was first derived to describe passive diffractive cavities [46], and later on, in the context of wave-guide dispersive cavities such as fiber cavities [47], whispering gallery mode resonators [49], and integrated ring resonators [50]. This equation has been also derived in the context of left-handed materials [51], for a chain of coupled silver nanoparticles embedded in a glass [52], in coupled-waveguide resonators [53], and for extended Josephson junctions [54]. This model constitutes a paradigm for the study of various dynamical properties of laser fields confined in either difractive or dispersive

nonlinear optical cavities [6] such as the emergence of patterns [28, 55–58], the formation of LS and clusters of them [15, 25, 27–29, 55, 59–61], self-pulsating LS or breathers [14, 17, 25, 29], LSs excitability [15], and some other complex spatiotemporal dynamics such as spatiotemporal chaos [62–64] or rogue waves [65–68].

Considering the transformations $E = e_c A$, $\tau = \tau_c X$, and $t = t_c T$, Eq. (1) can be written in the dimensionless form

$$\partial_T A = -(1+i\Delta)A - i\eta_2\partial_X^2 A + i(1-f_R)|A|^2 A + if_R A(\mathsf{R}\otimes|A|^2) + S, \quad (3)$$

where $e_c = \sqrt{\alpha/\gamma L}$, $\tau_c = \sqrt{L|\beta_2|/2\alpha}$, and $t_c = t_R/\alpha$, and the normalized detuning, pump intensity, and group velocity dispersion coefficients read:

$$\Delta = \frac{\delta_0}{\alpha}, \qquad S = \sqrt{\frac{\theta\gamma L}{\alpha^3}}E_{in}, \qquad \eta_2 = \text{sign}(\beta_2).$$

In Eq. (3), $\otimes$ is the convolution between the intensity $|A|^2$, and the extended Raman kernel R

$$\mathsf{R}(X) \equiv H(X)\cdot R'(X) \equiv H(X)\cdot \eta e^{-aX}\sin(bX), \quad (4)$$

where H is the Heaviside function, and

$$\eta = \tau_c\frac{\tau_1^2+\tau_2^2}{\tau_1\tau_2^2}, \qquad a = \tau_c/\tau_2, \qquad b = \tau_c/\tau_1.$$

The SRS term is calculated through the convolution theorem which states

$$\mathsf{R}\otimes|A|^2 = \mathcal{F}^{-1}(\mathcal{F}[\mathsf{R}]\cdot\mathcal{F}[|A|^2]),$$

where $\mathcal{F}$ is the Fourier transform. The real and imaginary parts of $\mathcal{F}[\mathsf{R}]$ read

$$\text{Re}(\mathcal{F}[\mathsf{R}]) = b\eta(a^2+b^2-k^2)/Z(k), \quad (5a)$$

$$\text{Im}(\mathcal{F}[\mathsf{R}]) = 2\eta abk/Z(k), \quad (5b)$$

with $Z(k) = (a^2+b^2-k^2)^2 + 4a^2k^2$. The imaginary part of $\mathcal{F}[\mathsf{R}]$ corresponds to the Raman gain spectrum, while the real one represents the modification of the refractive index due to the SRS term [69].

The SRS introduces an additional dependency on τ_c which becomes an important parameter for controlling the strength of the Raman response function R, and furthermore connects to physical parameters of the cavity such as chromatic dispersion coefficient, length and losses [40, 43]. The modification of the SRS response with τ_c is plotted in Fig. 2(a) for $\tau_c = 2, 5, 10$, and 20 fs, and $\text{Re}(\mathcal{F}[\mathsf{R}])$ and $\text{Im}(\mathcal{F}[\mathsf{R}])$ are shown in Fig. 2(b) and (c), respectively. While the envelope of R decreases with τ_c, the wavelength increases [see Fig. 2(a)], and when τ_c is very large, (i.e., $\tau_c \to \infty$), R becomes very sharp approaching an instantaneous response (i.e., a Dirac delta).

In the absence of SRS, Eq. (3) is invariant under the transformation $X \to -X$ (i.e., $X-$reflection symmetry), and its LS solutions normally preserve this symmetry. In contrast, when SRS is taken into account, the reflection symmetry is broken, leading to asymmetric solutions which now drift at a constant velocity v, which depends on the SRS control parameters [43].

In what follows, we focus on the normal dispersion regime (i.e., $\eta_2 = 1$), and we fix $f_R = 0.18$, $\tau_1 = 12.2$ fs, and $\tau_2 = 32$ fs corresponding to the common parameters of fused-silica based fibers [48]. With these specifications the main control parameters of the system are Δ, S and τ_c. Furthermore, in this work we consider a normalized domain width $l = 100$ and periodic boundary conditions.

III. CONTINUOUS WAVE BI-STABILITY AND DOMAIN WALLS DYNAMICS

The stationary states (i.e., $\partial_t A = 0$) of this system are described by

$$-(1+i\Delta)A + v\partial_X A - i\eta_2\partial_X^2 A + i(1-f_R)|A|^2 A + if_R A(\mathsf{R}\otimes|A|^2) + S = 0, \quad (6)$$

where we have considered the comoving frame transformation $X \to X - vT$, to take into account moving states at constant speed v.

The basic state solutions of Eq. (6) are the homogeneous or CW states A_h satisfying

$$I_h^3 - 2\Delta I_h^2 + (1+\Delta^2)I_h = S^2, \quad (7)$$

where $I_h \equiv |A_h|^2$. For $\Delta < \sqrt{3}$ A_h is single-valuate. For $\Delta > \sqrt{3}$, A_h is three-valuate, and therefore compose by the three solutions A_b, A_m and A_t, separated by two folds or saddle-node bifurcations $\text{SN}_{t,b}$ occurring at

$$I_{t,b} = \frac{2\Delta}{3} \pm \frac{1}{3}\sqrt{\Delta^2-3}. \quad (8)$$

In the later case, CW shows a hysteresis loop like the one plotted in Fig. 3 (top panel) for $\Delta = 4$. In the absence of SRS ($f_R = 0$), the middle branch A_m is always spatiotemporally unstable, the top one A_t is always stable, and the bottom one A_b undergoes a modulational instability (MI) at $(S_c, I_c) \equiv (\sqrt{(1+(1-\Delta)^2)}, 1)$ such that it is stable for $S < S_c$, and unstable between the MI and SN_b. We plot stable (unstable) solution branches using solid (dashed) lines. In the range between SN_t and MI (S_c) (see light red area in Fig. 3) stable A_b and A_t coexist, and in the following we refer to this interval as the *bi-stability* region.

Within the bi-stability region, DWs connecting A_t and A_b either upwards (DW_u) or downwards (DW_d) can form (see the inset in Fig. 3). DW_u and DW_d are related by a reflection $X \to -X$ respect to their center, i.e., $\text{DW}_u(X) = \text{DW}_d(-X)$, and in general, are not stationary, but move at constant speed and opposite direction depending on the parameters of the system.

To have some insight about the DWs behavior let us first show how an initial condition of the form

$$g^{b(t)}(X) = A_{b(t)} \pm he^{-[X/\sigma]^{10}}, \quad (9)$$

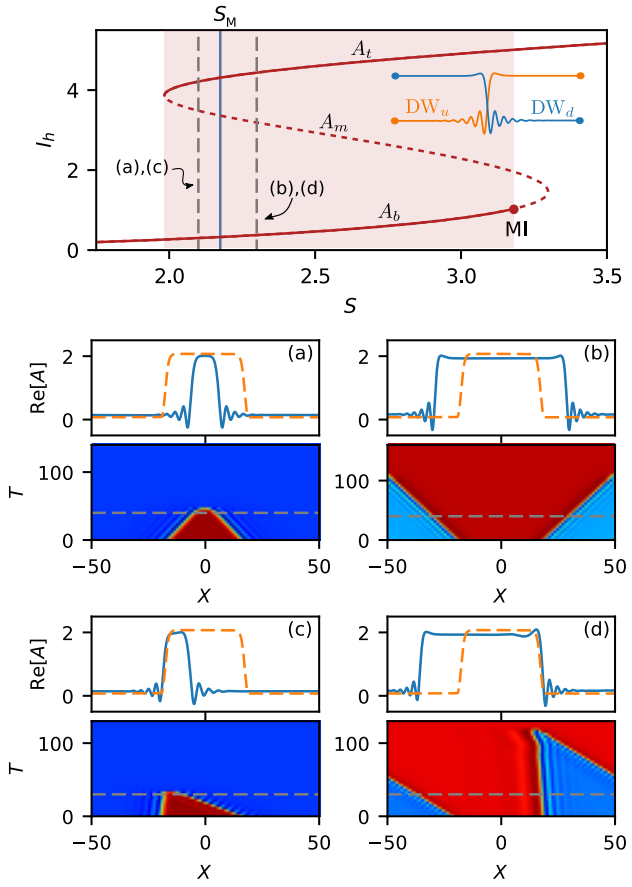


FIG. 3. Intensity of the CW state as a function of S for $\Delta = 4$. Stable (unstable) branches are shown with solid (dashed) lines. The light red area shows the bi-stability region. The blue vertical line corresponds to the Maxwell point of the system S_M, and the two vertical dashed gray lines correspond to the temporal evolutions shown in panels (a)-(d). Panels (a) and (b) show the evolution of two different initial conditions of the form $g^b(X)$ in the absence of SRS. Panels (c) and (d) show the temporal evolution of the same initial condition in the presence of SRS for $\tau_c = 5$ fs. The gray horizontal line on the colormaps corresponds to the blue profile on top of them.

composed by a super-Gaussian profile sitting on A_h evolves in time, with σ and h being its standard deviation and height. Figure 3(a) shows the evolution of Eq. (9) for $S = 2.1 < S_M$, and corresponds to the dashed gray line in the CW diagram. The g^b profile [see orange dashed line in Fig. 3(a,top)] establishes a connection between A_b and A_t, leading to the formation of DW$_u$ and DW$_d$, which soon after move inwards, with the same speed and opposite propagation direction. Eventually, the DWs annihilate one another, bringing the system back to A_b. A profile along such evolution is shown in Fig. 3(a,top) for $T = 40$.

Figure 3(b) shows the evolution of the same initial condition for $S = 2.3 > S_M$. For this value of S, the DWs move outwards, and eventually they meet at the boundaries of the domain, where they collide and disappear, such that the system terminates at the A_t state. The transition between these two scenarios takes place at the Maxwell point S_M of the system (see Fig. 3) where the DWs velocity cancels out [26, 70].

When the SRS is taken into account ($f_R \neq 0$), the features and dynamics of DWs change. The SRS breaks the reflection symmetry of the system, and DWs are no more related by the transformation $X \to -X$ [i.e., DW$_u(X) \neq$ DW$_d(-X)$]. Due to this asymmetry, DW$_u$ and DW$_d$ now move at different speeds and opposite directions, leading to the asymmetric time evolution shown in Figs. 3(c) and (d). For $S = 2.1 < S_M$ [see Fig. 3(c)] DW$_u$ moves slower than DW$_d$, although they eventually collide bringing the system back to A_b. For $S = 2.3 > S_M$ [see Fig. 3(d)], DW$_u$ moves much faster than DW$_d$, but as before, their annihilation eventually takes place, and the system finally reaches A_t.

IV. FORMATION OF LOCALIZES STATES IN ABSENCE OF STIMULATED RAMAN SCATTERING

The temporal evolutions shown in Sec. III correspond to values of S far from the Maxwell point of the system, where DWs annihilate one another, leading to one of the CW attractors, either A_b or A_t. Close to the Maxwell point however, DWs may lock at certain separations leading to the formation LSs of different widths [25, 26, 43]. In this section, we illustrate this mechanism in the absence of SRS ($f_R = 0$), and later, in Sec. V, we show the implications that the SRS may have on the LSs formation, dynamics and stability.

IV.1. Locking of domain walls

Close to the Maxwell point of the system (e.g., for $S = 2.18$ in Fig. 3), two initial conditions $g^t(X)$ of different widths lead to the formation of two coexistent dark LSs like those shown in Fig. 4(a)-(b). The formation of these LSs and their coexistence is a well-understood phenomenon mediated by the interaction and locking of DWs [11, 25, 71, 72]. Let us briefly review this mechanism. In the absence of SRS, DW$_{u,d}$ profiles look like those shown schematically in Fig. 4(c). These DWs exhibit *monotonic tails* around A_t, and *oscillatory tails* about A_b. These tails can be asymptotically described by $A(X) = A_{b(t)} + \epsilon e^{\lambda X}$, where $\epsilon \ll 1$ and λ is a complex number, solution of the eigenvalue equation

$$\lambda^4 - (4I_h - 2\Delta)\lambda^2 + \Delta^2 + 3I_h^2 - 4\Delta I_h + 1 = 0. \quad (10)$$

Figure 4(c) shows the set of eigenvalues associated with A_b (left) and A_t (right). While the eigenvalues associated with A_t are composed by four purely real eigenvalues $(\pm Q_1, \pm Q_2)$, those associated with A_b are complex conjugates $(\pm Q \pm iK)$. In this context, the shape of the tails is determined by the slowest mode $e^{\lambda_i X}$, and therefore associated with the leading eigenvalue (i.e., the one with the smallest $|\lambda_i|$), that we label $\lambda_l^{t,b}$ [see ∘ in Fig. 4(c)].

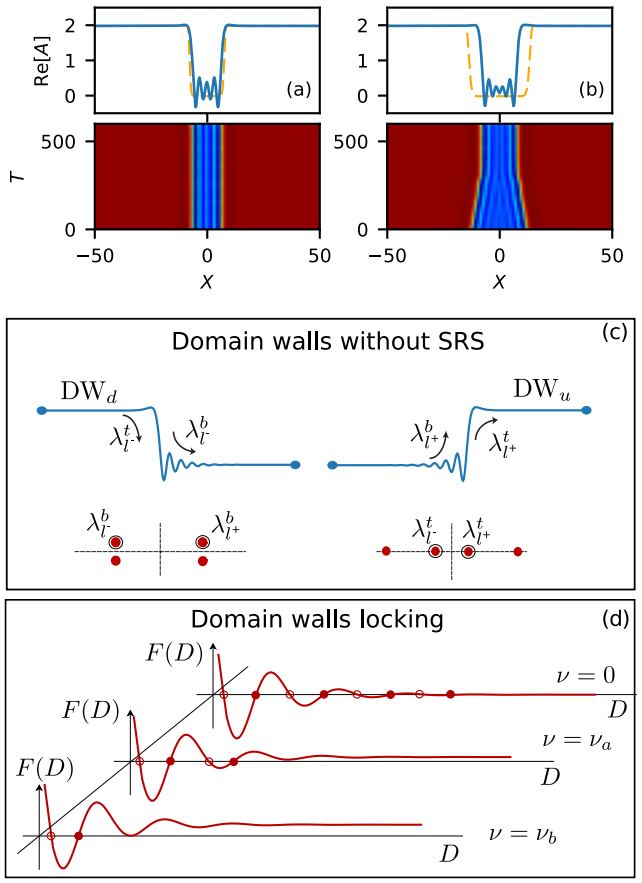


FIG. 4. Panels (a) and (b) show the formation of two different dark states starting from two distinct initial conditions. (c) shows a sketch of the profiles for DW$_u$ and DW$_d$, and the eigenvalues corresponding to each tail. In (d) we show schematically the function $F(D)$ [see Eq. (12)], defining the DWs locking, for three situations: at the Maxwell point ($\nu = 0$), and moving apart from it (ν_a and $\nu_b > \nu_a$).

Therefore, while the tail of DW$_d$ around A_t is asymptotically described by $\mathrm{DW}_d(X) - A_t \sim e^{\lambda^t_{l^-} X}$, the one around A_b is described by

$$\mathrm{DW}_d(X) - A_b \sim e^{\lambda^b_{l^-} X} = e^{-QX}\cos(KX), \tag{11}$$

with $Q = \mathrm{Re}[\lambda^b_{l^-}]$ and $K = \mathrm{Im}[\lambda^b_{l^-}]$.

Close to the Maxwell point S_M, the interaction of these DWs can be qualitatively described by the equation

$$\partial_t D = \varrho e^{QD}\cos(KD) + \nu \equiv F(D), \tag{12}$$

where D is the separation between DWs, $\nu \sim S - S_M$, ϱ is a positive constant depending on the system parameters [11, 71, 73, 74]. We have to point out that this equation cannot be explicitly derived from our model, and has been included here for illustrating the mechanism of DWs locking.

At S_M ($\nu = 0$) the fixed points of this equation $D^s_n = \frac{\pi}{2K}(2n+1)$, with $n = 0, 1, 2, \ldots$, correspond to the stationary distances at which the locking of DWs occurs [11, 71, 74]. Figure 4(d) shows these points and their stability using • for stable separations and ○ for unstable ones. If $S \neq S_M$, the stationary separations D^s_n are slightly modified by the factor ν, such that the more we increase the separation ν from S_M, the less LSs form, until eventually no more locking takes place. When the tails are monotonic ($K = 0$), two DWs attract each other until they annihilate one another in a process called coarsening [75].

The DWs studied here [see Fig. 4(c)] exhibit oscillatory tails around A_b, and are behind the formation of the dark LSs shown in Fig. 4(a)-(b). In contrast, the tails around A_t are monotonic, and therefore, no LSs form.

IV.2. Bifurcation structure for the dark localized states: Collapsed snaking

The dark LSs formed through this mechanism are organized in a bifurcation diagram like the one shown in Fig. 5, where we plot the L_2-norm

$$||A||^2 = \frac{1}{l}\int_{-l/2}^{l/2} |A(x)|^2 dx,$$

of the different steady states as a function of S. The red lines correspond to the CW states discussed in Sec. III, and the vertical dashed line marks the Maxwell point of the system S_M. We have computed this diagram fixing $\Delta = 4$, and performing a numerical parameter continuation on S based on a predictor-corrector method, as described in [76, 77].

The dark LSs formed through the locking of DWs undergo *collapsed snaking* [25, 72, 78, 79]: nearby S_M the LSs solution branches (see blue lines in Fig. 5) oscillate back and forth in S with an amplitude which decreases as descending in $||A||^2$. The labels (i)-(vi) correspond to the dark LSs of different widths shown on the right. While decreasing $||A||^2$ the LSs broaden as a result of the addition of tails wavelengths, until the DWs reach the domain width. At this stage, the solution branch, accumulated around S_M, leaves that point and connect back to the A_b CW branch at the MI (see Fig. 3) [25].

The stability of these states is marked using solid (dashed) lines for stable (unstable) states, and has been obtained by solving the eigenvalue problem

$$\mathcal{L}\psi = \sigma\psi,$$

where $\mathcal{L} = \mathcal{L}(A)$ is the linear operator associated with the right-hand side of Eq. (3) evaluated at a given LS, and σ and ψ are the eigenvalues and eigenmodes associated with $\mathcal{L}$. Note that we solve this problem numerically, and therefore, $\mathcal{L}$ corresponds to the Jacobian matrix obtained from the discretization of Eq. (3).

This bifurcation structure follows directly from the damped oscillatory DWs interaction described by Eq. (12). To understand this correspondence let us relate the sketch shown in Fig. 4(d) and the collapsed snaking of Fig. 5(a). At the Maxwell point S_M (i.e., for $\nu = 0$), a number stable and unstable dark LSs form at the stationary DWs separations D^s_n. Then the stable (unstable) LSs

in Fig. 4(d) correspond to a set of points on top of the stable (unstable) branches of solutions at S_M in Fig. 5(a).

When S separates from S_M [see Fig. 4(d) for $\nu = \nu_a$] less stationary separations D_n^s occur, resulting in the disappearance of solution branches corresponding to wider dark LSs. Increasing further the value of S [see Fig. 4(d) for $\nu = \nu_b$], only two intersections occur and only the stable and unstable single peak solution branches remain. Proceeding in this way eventually no more intersections take place, resulting in the complete disappearance of the LSs. Note that the SNs in the collapsed snaking occur at the tangencies shown in Fig. 4(d). For very large separations (i.e. small $||A||^2$) the interaction is very weak, and wide dark LS branches approach asymptotically the Maxwell point S_M.

Dark LSs persist for different values of Δ and undergo temporal oscillatory (i.e., Hopf) instabilities that make them breathe [25]. Figure 5(b) shows the phase diagram of these states in the $(\Delta, S)-$parameter space, where the first two folds of the dark LSs $\mathrm{SN}_D^{l,r}$ and the Hopf instability H are plotted. Within the light red area dark LSs undergo oscillatory dynamics, whereas in the light blue one they are stable. Increasing Δ, the region of existence of these regimes broadens. However, when decreasing Δ they shrink until eventually the different LSs disappear in a sequence of cusp bifurcations [25]. For simplicity here we only plot the cusp C_D associated with the dark state shown in the profile (i).

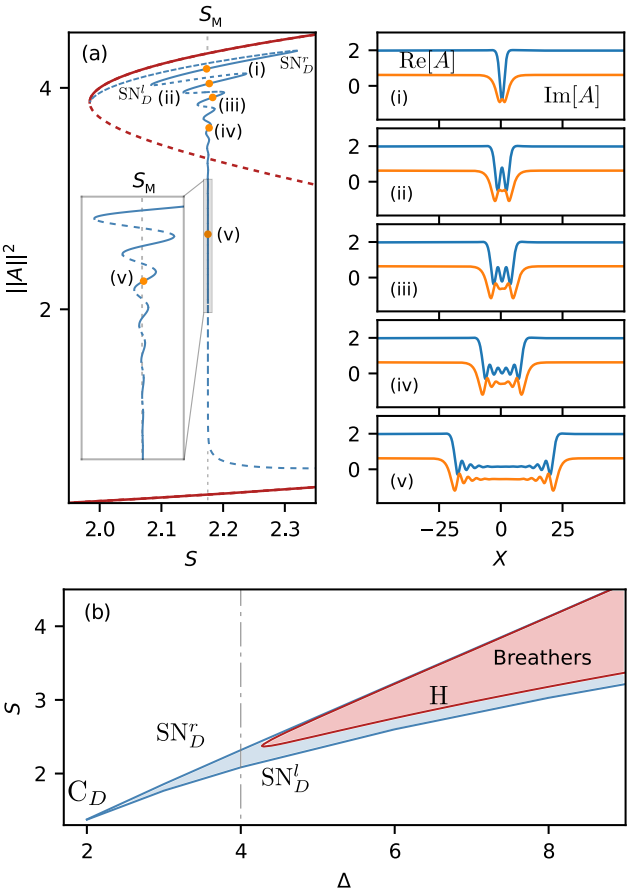


FIG. 5. Panel (a) shows the collapsed snaking bifurcation diagram (blue lines) for $\Delta = 4$ in the absence of SRS ($f_R = 0$). This diagram shows the norm $||A||^2$ of the different states as a function of S. The dark red lines represent the CW state. Stable (unstable) branches are shown with solid (dashed) lines. The labels (i)-(vi) correspond to the dark LSs shown on the right. Panel (b) shows the phase diagram in the $(\Delta, S)-$parameter space. The blue lines correspond to $\mathrm{SN}_D^{l,r}$, and the red ones to the Hopf bifurcation H.

V. COEXISTENCE OF BRIGHT AND DARK LOCALIZED STATES IN THE PRESENCE OF STIMULATED RAMAN SCATTERING

The dynamics, interaction and locking of DWs can be strongly modified by the influence of high-order dispersion effects [33], or long range interactions [73, 74, 80–84], such as SRS. Figure 6 shows the temporal evolution of different initial conditions of the form $g^{b,t}(X)$ in the presence of SRS. Panels 6(a) and (b) correspond to the evolution of two initial conditions $g^t(X)$ of different widths (see orange dashed profile) for $(\Delta, S) = (4, 2.21)$ and $\tau_c = 5$ fs. In both cases the initial condition converges fast to asymmetric dark LSs of different widths which drift at constant speed v (see blue profiles). Thus, as for the vanishing SRS case, different type of dark LSs coexist for a single value of S. For the same parameters, similar dynamical behaviors are observed starting with initial conditions of the form $g^b(X)$, as can be seen in Figs. 6(c) and (d). In this case, the system evolves to two moving bright states of different extensions, which were absent for vanishing SRS. Therefore, we can conclude that bright LSs are stabilized through SRS effect.

The formation of these bright states can be also explained in terms of DWs interaction and locking. Figure 6(e) shows the real part of DW_d and DW_u for the same parameter values used in the previous temporal simulations. Due to the SRS effect, the shape of the tails around either A_t and A_b differs from DW_d to DW_u, and, as we previously stated, $\mathrm{DW}_u(X) \neq \mathrm{DW}_d(-X)$. A close-up view of the tails of DW_d around A_t [see gray box in Fig. 6(e)] is shown in Fig. 6(f), where we also add the tails of the unperturbed case (i.e., $f_R = 0$) for comparison (see red dashed line). While in the unperturbed case the tail of DW_d leaves A_t monotonically (i.e., the dominant spatial eigenvalue has the form $\lambda_{l+}^t = +Q$), in the SRS case the tail leaves A_t in a damped oscillatory manner associated with an eigenvalue $\lambda_{l+}^t = +Q + iK$. This modification introduces a new way of interaction, such that the locking not only occurs around A_b, but also around A_t, leading to the formation of bright LSs. In this context, the characteristic time τ_c plays an important role on the modification of the DWs tails: decreasing τ_c the wavelength of the tails increases, while its decaying weakens. This behavior is captured in Fig. 6(f) where we compare the shape of the tail for $\tau_c = 5$ fs (blue line) and $\tau_c = 2$ fs (orange line). Note that similar tail modifications take place in the presence of other terms

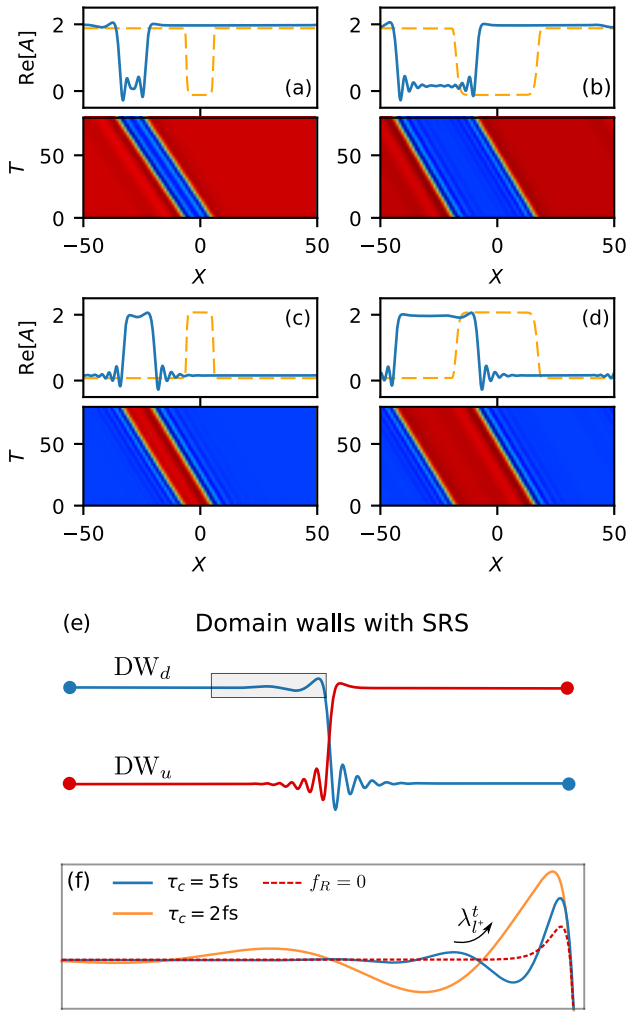


FIG. 6. Formation of LSs in the presence of SRS for $\Delta = 4$, $S = 2.21$, and $\tau_c = 5$ fs. Panels (a)-(b) show the formation and temporal evolution of dark LSs starting from two different initial conditions (see yellow dashed line). Panels (c)-(d) show the formation and evolution of bright LSs starting from different initial conditions than in (a) and (b). In (e) we plot schematically two DWs profiles corresponding to DW$_d$ in blue and DW$_u$ in red. The gray area highlights the oscillatory tails around A_t plotted in detail in the close-up view of panel (f). For comparison panel (f) also shows the tails when $\tau_c = 2$ fs (orange line), and in the absence of SRS (red dashed line).

breaking $X-$reflection symmetry such as third-order dispersion [33, 35].

Close to the nascent bistability onset, an equation describing the DWs interaction can be derived [43, 45]. In that limit, the resulting equation shows that the interaction and DWs locking depends on the balance between two factors: i) a contribution due to the DWs tails, and ii) a contribution directly related to the long-range interaction (see Eq. (7) in [43]). One could expect that such dependence might persist in the full model (3), with the oscillatory tails contribution to the interaction being described by Eq. (12). However, the explicit derivation of an interaction equation in this context, if possible, might not be straightforward, and it is beyond the scope of the present work.

VI. BIFURCATION STRUCTURE FOR RAMAN DARK AND BRIGHT LOCALIZED STATES

As we have already mentioned in Sec. III, the collapsed snaking is determined by the damped oscillatory nature of the DWs tails through Eq. (12). Therefore, any modification of the DWs tails and/or features of the interaction law, like the ones induced by the SRS, may change the LSs bifurcation structure.

Figure 7 shows the modification of the collapsed snaking diagram for $\Delta = 4$ in the presence of SRS when $\tau_c = 5$ fs. The labels (i)-(viii) mark the position of the LSs shown on the right. Due to the $X \to -X$ symmetry breaking these LSs drift at constant speed v and are solutions of Eq. (6). To compute these states and track them numerically in a given parameter, we need to consider a phase condition of the form $C[A] = 0$ to take account for the LSs speed. Here, we define this condition as the constraint $C[A] = d\mathrm{Re}[A]/dX|_{X_0} = 0$ which forces one extremum of the LS (maximum or minimum) to be located at $X = X_0$ [32, 33]. In this manner, the speed of the LSs is computed as a part of the solution in the continuation algorithm. Figures 7(b)-(c) show the computed speed as a function of the LSs width D. The inner sub-panels in Fig. 7(a) show a close-up view of the top and bottom part of the bifurcation diagram, which allows us to illustrate better the organization of those solution branches.

The top part of the diagram corresponds to the solution branches associated with the dark LSs presented in Sec. IV. Due to the effect of the SRS, these states are now asymmetric as shown in Fig. 7(i)-(iv). Note that the complex form of this part of the diagram may be related to an interaction and locking process more complicated than the one described in Sec. IV. However, the confirmation of this scenario requires further investigation. The velocity of these states is not constant [see Fig. 7(b)] but oscillates with D, and therefore along the diagram shown in Fig. 7(a). For $D \lesssim 20$ the velocity shows large oscillations with D which correspond to dark states with higher $||A||^2$. For $D \gtrsim 20$ (i.e., decreasing in $||A||^2$), the LSs collapse to the Maxwell point, and so does the velocity which saturates to an almost constant value.

The bottom part of the diagram shows a regular collapsed snaking in S, which is absent when $f_R = 0$ [see Fig. 5(a)]. This new bifurcation structure is related to the locking of DWs around A_t, which is now possible due to the presence of oscillatory tails about such state, and the presence of the long range interaction (see Sec. V)[43]. Four representative LS examples along this part of the diagram are shown in Fig. 7(v)-(viii). These asymmetric bright LSs drift at constant speed, whose damped oscillatory dependence with S is plotted Fig. 7(c).

Dark and bright LSs persist for different values of Δ as shown in the phase diagram of Figure 8, where we show

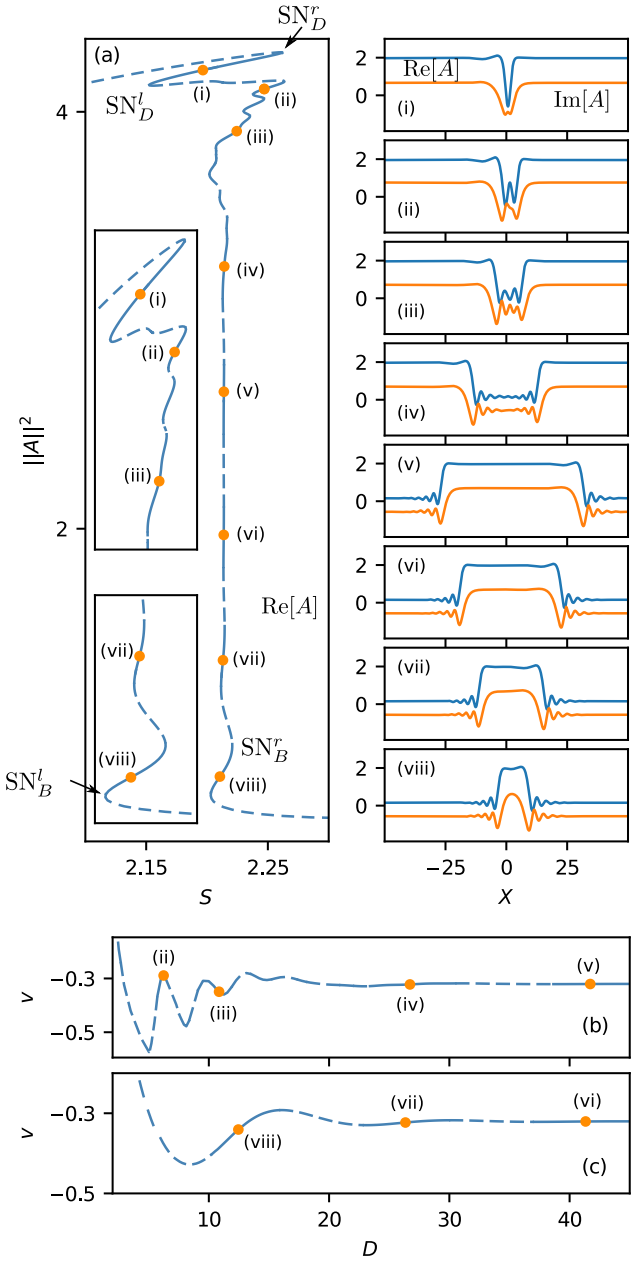


FIG. 7. Panel (a) shows the LSs bifurcation diagram for $\Delta = 4$ in the presence of SRS with $\tau_c = 5$ fs. The labels (i)-(viii) correspond to the LSs shown on the right. Stable (unstable) solution branches are marked using solid (dashed) lines. Panel (b) shows the velocity of dark LSs as a function of their width D. In (c) the same than in (b) for the case of bright LSs.

the main bifurcation lines of the system. This diagram has been computed through a two-parameter continuation in (Δ, S) while fixing $\tau_c = 5$ fs. As in Fig. 5(b) the blue lines correspond to the first two folds of the single dip dark LS $\mathrm{SN}_D^{l,r}$, the red line is the Hopf bifurcation undergone by these states, and in orange we plot the first two folds of the bright LSs, namely $\mathrm{SN}_B^{l,r}$ [see Fig. 7(a)]. The dashed gray lines correspond to $\mathrm{SN}_D^{l,r}$ in the absence of SRS (i.e., $f_R = 0$), and have been added for comparison. The vertical pointed-dashed line corresponds to the bifurcation diagram shown in Fig. 7 for $\Delta = 4$, and the dashed one to Fig. 9.

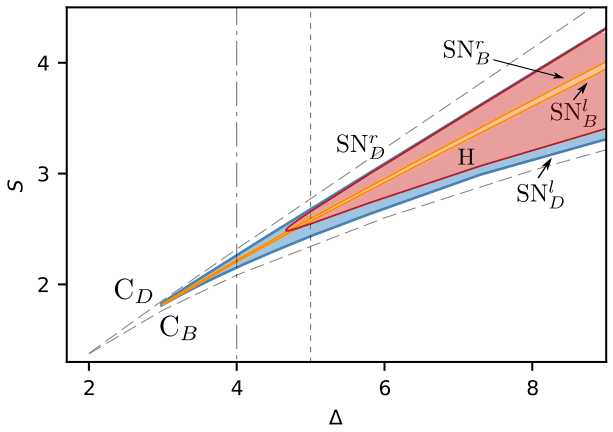


FIG. 8. Phase diagram in the $(\Delta, S)-$parameter space showing the main bifurcation lines of the system in the presence of SRS ($f_R \neq 0$) for $\tau_c = 5$ fs: $\mathrm{SN}_D^{l,r}$ (blue lines) are the first two folds of the dark states, $\mathrm{SN}_B^{l,r}$ (orange lines) are the first two folds of the bright LSs, and H (red line) corresponds to the Hopf bifurcation. The dashed gray lines correspond to $\mathrm{SN}_D^{l,r}$ in the absence of SRS, and vertical point-dashed and dashed vertical ones to the bifurcation diagrams shown in Figs. 7 and 9 respectively.

In the presence of SRS, the different dynamical regions shown in Fig. 5(b), such as the region of existence of single dip dark LSs and the breathing region shrink, leading in this way to a partial stabilization of the previous breathing dark states. The area in-between $\mathrm{SN}_B^{l,r}$ (see light orange area) shows the region of existence of the bright LSs, which widens increasing Δ. Decreasing Δ, however, this region shrinks until eventually SN_D^l and SN_D^r collide and disappear in a cusp bifurcation C_B, which occurs approximately for the same values than C_D.

Figure 9 shows the bifurcation diagram for $\Delta = 5$. For this value of Δ the bottom of the diagram is very much alike the one shown in Fig. 7 for $\Delta = 4$, and some representative examples of bright LSs are shown in panels 9(i)-(iv). The top part of the diagram, however, although morphologically similar to the one depicted in Fig. 7, undergoes a Hopf instability (see close-up view in the inset of Fig. 9), that makes the single dip dark state [see profile (vi)] breathe as shown in Fig. 9(vii).

The collapsed snaking bifurcation structure, and the instabilities undergone by their underlying LSs persist for higher values of Δ as shown in the phase diagram of Fig. 8. Note that bright LSs may also undergo oscillatory instabilities [44]. However, for the range of parameters studied in this work we have not observed such type of dynamics.

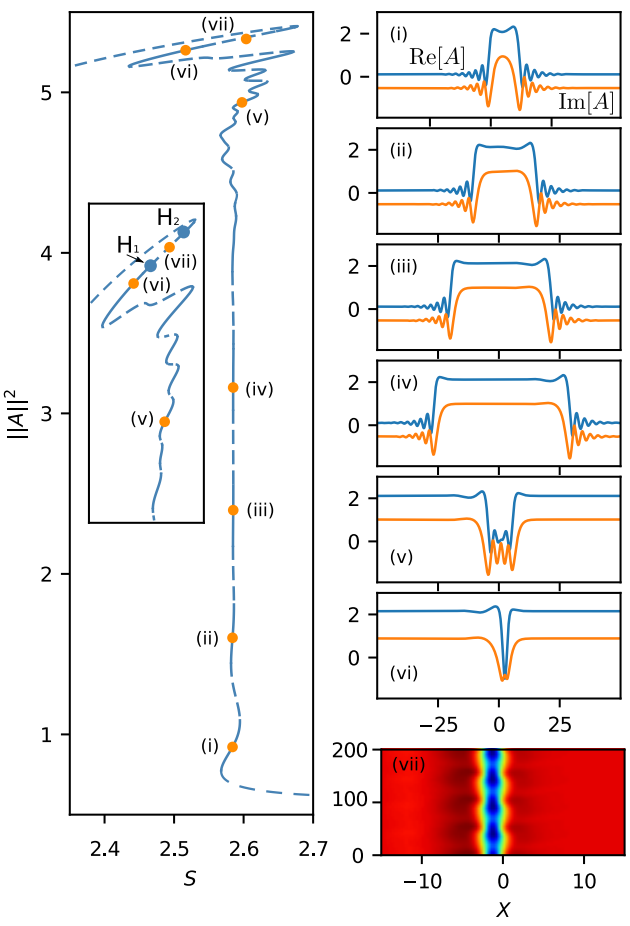


FIG. 9. Collapsed snaking for $\Delta = 5$ and $\tau_c = 5$ fs corresponding to the dashed vertical line shown in Fig. 8. The labels (i)-(vi) correspond to the LSs shown on the right, and panel (vii) shows the evolution of a breather within several oscillatory periods.

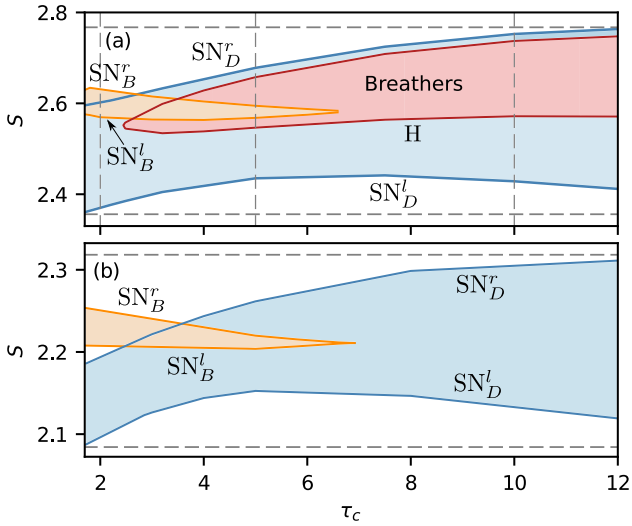


FIG. 10. Panel (a) shows the $(\tau_c, S)-$phase diagram for $\Delta = 5$, where the main bifurcations of the system are plotted: $\mathrm{SN}_D^{l,r}$ (blue lines) are the first two fold of the dark states, $\mathrm{SN}_B^{l,r}$ (orange lines) are the first two folds of the bright LSs, and H (red line) corresponds to the Hopf bifurcation. The vertical lines in panel (a) corresponds to the bifurcation diagrams shown in Fig. 11. Panel (b) shows the same type of phase diagram for $\Delta = 4$. In both panels horizontal dashed lines represent the position of $\mathrm{SN}_D^{l,r}$ for vanishing SRS.

VII. INFLUENCE OF τ_c ON THE LOCALIZED STATES DYNAMICS AND STABILITY

So far we have studied the influence of the SRS on the dynamics and stability of LSs for a single value of the characteristic time $\tau_c = 5$ fs. This parameter strongly impacts the stability of LSs as shown in the context of anomalous dispersion [40], and one may wonder how the previous scenario modifies when varying its value.

To clarify this point we perform a two-parameter continuation of the main bifurcations of the system in S and τ_c by fixing Δ. The outcome of these computations is shown in Fig. 10 for two different values of detuning Δ. In Fig. 10(a) we show the $(\tau_c, S)-$phase diagram for $\Delta = 5$, and Fig. 10(b) shows the one for $\Delta = 4$. In both cases the horizontal dashed lines mark the position of $\mathrm{SN}_D^{l,r}$ in the absence of SRS for comparison. Note that the Hopf bifurcation H is present for $\Delta = 5$ [see red line line in Fig. 10(a)], while absent for $\Delta = 4$ [see Fig. 10(b)].

For $\Delta = 5$, the modification of the collapsed snaking structure with τ_c is depicted in Fig. 11 for three particular values of τ_c corresponding to the vertical dashed lines shown in Fig. 10(a). For $\tau_c = 10$ fs [see Fig. 11(a)] the scenario is very similar to the unperturbed case (see gray diagram computed for $f_R = 0$), although the Hopf instability slightly modifies its position as shown in the close-up view of Fig. 11(a). In addition, the collapsed snaking corresponding to the bottom of the diagram is strongly compressed. Increasing τ_c further, the Raman response function R becomes sharper and highly damped (see Sec. II) tending to an almost instantaneous response, and therefore, the deviation from the unperturbed case is almost negligible.

Reducing τ_c, however, the SRS modifies strongly the DWs tails (see Sec. V), and as a consequence the LSs bifurcation structure. Thus, while the region of existence of dark LSs and breathers shrinks, the region of existence of bright LSs broadens [see phase diagram in Fig. 10(a)]. An example of this situation is shown in Fig. 11(b) for $\tau_c = 5$ fs, where whereas the top part of the diagram is highly modified (see close-up view), the bottom one shows larger damped oscillations in S as a result of the appearance of bright LSs like the one shown in Fig. 11(i).

Decreasing τ_c even further, the Hopf bifurcation disappears, and with it, the breathing behavior [see Fig. 10(a)], leading to the stabilization of the single dip dark states. In this regime the bifurcation structure is similar to the one depicted in Fig. 11(c) for $\tau_c = 2$ fs. For this value of τ_c the branches corresponding to the dark states are strongly modified [see the detailed view in the inset of panel 11(c)], and the bright LSs increase their region of existence due to the dominant interaction of the DWs

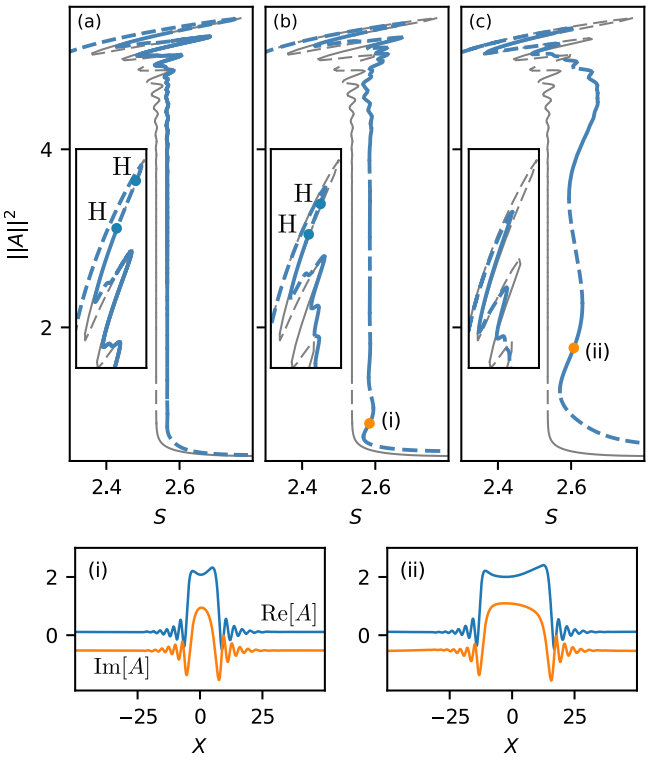


FIG. 11. Modification of the collapsed snaking structure for $\Delta = 5$ while increasing τ_c (see blue diagram): in (a) $\tau_c = 10$ fs, in (b) $\tau_c = 5$ fs, and in (c) $\tau_c = 2$ fs. In gray we have also plotted the diagram in the absence of SRS for comparison. The inset panels show a close-up view of the top part of the collapsed snaking where the Hopf instabilities H are signaled. Two examples of bright LSs profiles are plotted in sub-panels (i) and (ii).

tails around A_t. An example of this type of bright LSs is shown in panel 11(ii). For $\Delta = 4$ [see Fig. 10(b)] the scenario is quite similar to the previous one, despite of the absence of the breather regime.

VIII. DISCUSSION AND CONCLUSIONS

We have presented a detailed theoretical study of the dynamics and bifurcation structure of dissipative LSs emerging in externally driven Kerr cavities in the presence of stimulated Raman scattering. To perform this study we have considered the modified Lugiato-Lefever equation with the Raman response, and we have focused on the normal group velocity dispersion regime (see Sec. II).

In the absence of SRS, the typical LSs arising in this regime are dark. These type of LSs form due to the locking of DWs which exist within a region of bi-stability between two different CW states. The locking occurs through the overlapping of the DWs tails leading to LSs of different extensions that can be seen as a portion of one CW state embedded on the other one (see Sec. III and IV). From a bifurcation perspective and a fixed value of Δ, these states undergo *collapsed snaking* (see Sec. IV): the LSs solution branches experience a sequence of exponentially decaying oscillations in the pump S around the Maxwell point of the system, as a result of the DWs interaction and locking [25, 26, 72]. For large values of detuning Δ, moreover, these states undergo oscillatory instabilities that make them breathe [25, 26].

The presence of SRS strongly modifies the dynamics and stability of the previous states, and furthermore induces the emergence of bright LSs [43]. From a dynamical point of view, the SRS effect has two main implications. First, the SRS term breaks the reflection symmetry $X \to -X$, inducing a constant drift in the, otherwise static, LSs. Second, the SRS modifies the spatial eigenvalues of the CW states (i.e., the shape of the DWs oscillatory tails), and the interaction and locking of DWs. As a result of this alteration, the dark states modify their dynamics, and bright LSs arise (see Sec. V).

Note that the drift can be also induced by other mechanisms such as odd chromatic dispersion effects [31–33, 61], phase gradients [85], and external delay feedback [86, 87], among others [88–90].

Dark and bright Raman LSs undergo collapsed snaking that we have characterized in detail as a function of Δ and S for a fixed value of the characteristic time parameter τ_c. Figure 8 in Sec. VI summarizes the main dynamical regimes in the $(\Delta, S)-$phase space for $\tau = 5$ fs. As shown in [40, 43], the parameter τ_c has important implications regarding the LSs stability. These implications have been analyzed in detail in Sec. VII, and the main results are summarized in Fig. 10. The larger the value of τ_c, the stronger the SRS effect and modification of the DW tails, resulting in a more complex collapsed snaking structure (see Fig. 11). Note that $\tau_c = \sqrt{L|\beta_2|/2\alpha}$, and we can reinterpret the previous results in terms of the cavity length L, losses α, and chromatic dispersion coefficient β_2. Thus, if we fix L and α, $\tau_c \propto \sqrt{|\beta_2|}$, and we can reformulate the conclusion of Sec. VII in terms of β_2. Therefore, whereas increasing β_2 the existence region of dark LSs and breathers widens, the one of bright LSs shrinks, and eventually disappears.

A similar scenario, also supported experimentally, can be found when the $X-$reflection symmetry is broken through third order chromatic dispersion [33, 91]. In such case, the modification of the DWs tails about A_b is much more prominent than in the presence of SRS, and as a consequence, the existence region of bright LSs is much wider. Furthermore, the extension of this region increases with the strength of the third order dispersion, in contrast to the SRS case where it decreases with τ_c.

This work has been performed for a fixed domain width $l = 100$, although the results presented here can be generalized to different domain extensions. As the LSs width is an integer multiple of the DWs tails wavelength, the size of the domain can strongly constraint the variety of LSs allowed in the system. Thus, the larger the domain (i.e., the cavity), the wider the states that can emerge in the system. Some physical parameter values of all fiber cavities, for which the observation of these type of struc-

tures may be possible, are presented in [43].

In conclusion, we have shown that SRS strongly impacts the LSs formation, dynamics, stability, and bifurcation structure in the bi-stability scenario typical of the normal dispersion regime. The modifications and features of this scenario have been analyzed and characterized in detail. We have shown that Raman dark and bright LSs are robust, and persist under modification of different control parameters of the system.

The final aim of studies of this kind is to be useful for understanding the formation and dynamics of LSs in Kerr nonlinear optical cavities, and guiding experiments in this type of systems, as has been done previously [20, 91].

ACKNOWLEDGMENTS

PPR and MT acknowledge support from the Fonds National de la Recherche Scientifique F.R.S.-FNRS, (Belgium). SC acknowledges the LABEX CEMPI (ANR-11-LABX-0007) as well as the Ministry of Higher Education and Research, Hauts de France council and European Regional Development Fund (ERDF) through the Contract de Projets Etat-Region (CPER Photonics for Society P4S). MC acknowledges funding from Millennium Institute for Research in Optics (MIRO) and FONDECYT projects 1180903.

[1] G. Nicolis and I. Prigogine, *Self-organization in nonequilibrium systems: from dissipative strfuctures to order through fluctuations*. New York, N.Y.: Wiley, 1977.
[2] M. C. Cross and P. C. Hohenberg, "Pattern formation outside of equilibrium," *Reviews of Modern Physics*, vol. 65, pp. 851–1112, July 1993.
[3] N. Akhmediev and A. Ankiewicz, eds., *Dissipative Solitons*. Lecture Notes in Physics, Berlin Heidelberg: Springer-Verlag, 2005.
[4] N. Akhmediev and A. Ankiewicz, *Dissipative solitons: from optics to biology and medicine*. Lecture Notes in Physics, Berlin Heidelberg: Springer-Verlag, 2008.
[5] O. Descalzi, M. G. Clerc, S. Residori, and G. Assanto, eds., *Localized States in Physics: Solitons and Patterns*. Berlin Heidelberg: Springer-Verlag, 2011.
[6] Y. K. Chembo, D. Gomila, M. Tlidi, and C. R. Menyuk, "Theory and applications of the lugiato-lefever equation," 2017.
[7] M. Tlidi, M. G. Clerc, and K. Panajotov, "Dissipative structures in matter out of equilibrium: from chemistry, photonics and biology, the legacy of Ilya Prigogine (part 2)," *Philosophical Transactions of the Royal Society A: Mathematical, Physical and Engineering Sciences*, vol. 376, p. 20180276, Dec. 2018.
[8] M. Tlidi, M. G. Clerc, and K. Panajotov, "Dissipative structures in matter out of equilibrium: from chemistry, photonics and biology, the legacy of Ilya Prigogine (part 1)," *Philosophical Transactions of the Royal Society A: Mathematical, Physical and Engineering Sciences*, vol. 376, p. 20180114, July 2018.
[9] B. A. Malomed and D. Mihalache, "Nonlinear waves in optical and matter-wave media: A topical survey of recent theoretical and experimental results," *Rom. J. Phys*, vol. 64, p. 106, 2019.
[10] L. Lugiato, F. Prati, M. Gorodetsky, and T. Kippenberg, "From the lugiato–lefever equation to microresonator-based soliton kerr frequency combs," *Philosophical Transactions of the Royal Society A: Mathematical, Physical and Engineering Sciences*, vol. 376, no. 2135, p. 20180113, 2018.
[11] P. Coullet, "Localized patterns and fronts in nonequilibrium systems," *International Journal of Bifurcation and Chaos*, vol. 12, pp. 2445–2457, Nov. 2002.
[12] A. J. Scroggie, W. J. Firth, G. S. McDonald, M. Tlidi, R. Lefever, and L. A. Lugiato, "Pattern formation in a passive Kerr cavity," *Chaos, Solitons & Fractals*, vol. 4, pp. 1323–1354, Aug. 1994.
[13] W. J. Firth and A. Lord, "Two-dimensional solitons in a Kerr cavity," *Journal of Modern Optics*, vol. 43, pp. 1071–1077, May 1996.
[14] W. J. Firth, G. K. Harkness, A. Lord, J. M. McSloy, D. Gomila, and P. Colet, "Dynamical properties of two-dimensional kerr cavity solitons," *JOSA B*, vol. 19, no. 4, pp. 747–752, 2002.
[15] D. Gomila, M. A. Matas, and P. Colet, "Excitability Mediated by Localized Structures in a Dissipative Nonlinear Optical Cavity," *Physical Review Letters*, vol. 94, p. 063905, Feb. 2005.
[16] F. Leo, S. Coen, P. Kockaert, S.-P. Gorza, P. Emplit, and M. Haelterman, "Temporal cavity solitons in one-dimensional Kerr media as bits in an all-optical buffer," *Nature Photonics*, vol. 4, pp. 471–476, July 2010.
[17] F. Leo, L. Gelens, P. Emplit, M. Haelterman, and S. Coen, "Dynamics of one-dimensional Kerr cavity solitons," *Optics Express*, vol. 21, pp. 9180–9191, Apr. 2013.
[18] T. Herr, V. Brasch, J. D. Jost, C. Y. Wang, N. M. Kondratiev, M. L. Gorodetsky, and T. J. Kippenberg, "Temporal solitons in optical microresonators," *Nature Photonics*, vol. 8, pp. 145–152, Feb. 2014.
[19] X. Xue, Y. Xuan, Y. Liu, P.-H. Wang, S. Chen, J. Wang, D. E. Leaird, M. Qi, and A. M. Weiner, "Mode-locked dark pulse Kerr combs in normal-dispersion microresonators," *Nature Photonics*, vol. 9, pp. 594–600, Sept. 2015.
[20] B. Garbin, Y. Wang, S. G. Murdoch, G.-L. Oppo, S. Coen, and M. Erkintalo, "Experimental and numerical investigations of switching wave dynamics in a normally dispersive fibre ring resonator," *The European Physical Journal D*, vol. 71, p. 240, Sept. 2017.
[21] P. DelHaye, A. Schliesser, O. Arcizet, T. Wilken, R. Holzwarth, and T. J. Kippenberg, "Optical frequency comb generation from a monolithic microresonator," *Nature*, vol. 450, pp. 1214–1217, Dec. 2007.
[22] T. J. Kippenberg, R. Holzwarth, and S. A. Diddams, "Microresonator-Based Optical Frequency Combs," *Science*, vol. 332, pp. 555–559, Apr. 2011.

[23] A. Pasquazi, M. Peccianti, L. Razzari, D. J. Moss, S. Coen, M. Erkintalo, Y. K. Chembo, T. Hansson, S. Wabnitz, P. DelHaye, X. Xue, A. M. Weiner, and R. Morandotti, "Micro-combs: A novel generation of optical sources," *Physics Reports*, vol. 729, pp. 1–81, Jan. 2018.

[24] S. Coen, M. Tlidi, P. Emplit, and M. Haelterman, "Convection versus Dispersion in Optical Bistability," *Physical Review Letters*, vol. 83, pp. 2328–2331, Sept. 1999.

[25] P. Parra-Rivas, E. Knobloch, D. Gomila, and L. Gelens, "Dark solitons in the Lugiato-Lefever equation with normal dispersion," *Physical Review A*, vol. 93, p. 063839, June 2016.

[26] P. Parra-Rivas, D. Gomila, E. Knobloch, S. Coen, and L. Gelens, "Origin and stability of dark pulse Kerr combs in normal dispersion resonators," *Optics Letters*, vol. 41, pp. 2402–2405, June 2016.

[27] D. Gomila, A. J. Scroggie, and W. J. Firth, "Bifurcation structure of dissipative solitons," *Physica D: Nonlinear Phenomena*, vol. 227, pp. 70–77, Mar. 2007.

[28] P. Parra-Rivas, D. Gomila, L. Gelens, and E. Knobloch, "Bifurcation structure of localized states in the Lugiato-Lefever equation with anomalous dispersion," *Physical Review E*, vol. 97, p. 042204, Apr. 2018.

[29] P. Parra-Rivas, D. Gomila, M. A. Matas, S. Coen, and L. Gelens, "Dynamics of localized and patterned structures in the Lugiato-Lefever equation determine the stability and shape of optical frequency combs," *Physical Review A*, vol. 89, p. 043813, Apr. 2014.

[30] M. Tlidi and L. Gelens, "High-order dispersion stabilizes dark dissipative solitons in all-fiber cavities," *Optics Letters*, vol. 35, pp. 306–308, Feb. 2010.

[31] M. Tlidi, L. Bahloul, L. Cherbi, A. Hariz, and S. Coulibaly, "Drift of dark cavity solitons in a photonic-crystal fiber resonator," *Physical Review A*, vol. 88, p. 035802, Sept. 2013.

[32] P. Parra-Rivas, D. Gomila, F. Leo, S. Coen, and L. Gelens, "Third-order chromatic dispersion stabilizes Kerr frequency combs," *Optics Letters*, vol. 39, pp. 2971–2974, May 2014.

[33] P. Parra-Rivas, D. Gomila, and L. Gelens, "Coexistence of stable dark- and bright-soliton Kerr combs in normal-dispersion resonators," *Physical Review A*, vol. 95, p. 053863, May 2017.

[34] V. E. Lobanov, A. V. Cherenkov, A. E. Shitikov, I. A. Bilenko, and M. L. Gorodetsky, "Dynamics of platicons due to third-order dispersion," *The European Physical Journal D*, vol. 71, p. 185, July 2017.

[35] J. H. Talla Mb, C. Milin, and Y. K. Chembo, "Existence and switching behavior of bright and dark Kerr solitons in whispering-gallery mode resonators with zero group-velocity dispersion," *The European Physical Journal D*, vol. 71, p. 196, July 2017.

[36] C. Milin, A. V. Gorbach, M. Taki, A. V. Yulin, and D. V. Skryabin, "Solitons and frequency combs in silica microring resonators: Interplay of the Raman and higher-order dispersion effects," *Physical Review A*, vol. 92, p. 033851, Sept. 2015.

[37] Y. K. Chembo, I. S. Grudinin, and N. Yu, "Spatiotemporal dynamics of Kerr-Raman optical frequency combs," *Physical Review A*, vol. 92, p. 043818, Oct. 2015.

[38] V. E. Lobanov, G. Lihachev, T. J. Kippenberg, and M. L. Gorodetsky, "Frequency combs and platicons in optical microresonators with normal GVD," *Optics Express*, vol. 23, pp. 7713–7721, Mar. 2015.

[39] X. Yi, Q.-F. Yang, K. Y. Yang, and K. Vahala, "Theory and measurement of the soliton self-frequency shift and efficiency in optical microcavities," *Optics Letters*, vol. 41, pp. 3419–3422, Aug. 2016.

[40] Y. Wang, M. Anderson, S. Coen, S. G. Murdoch, and M. Erkintalo, "Stimulated Raman Scattering Imposes Fundamental Limits to the Duration and Bandwidth of Temporal Cavity Solitons," *Physical Review Letters*, vol. 120, p. 053902, Jan. 2018.

[41] W. Chen, B. Garbin, A. U. Nielsen, S. Coen, S. G. Murdoch, and M. Erkintalo, "Experimental observations of breathing Kerr temporal cavity solitons at large detunings," *Optics Letters*, vol. 43, pp. 3674–3677, Aug. 2018.

[42] A. V. Cherenkov, N. M. Kondratiev, V. E. Lobanov, A. E. Shitikov, D. V. Skryabin, and M. L. Gorodetsky, "Raman-Kerr frequency combs in microresonators with normal dispersion," *Optics Express*, vol. 25, pp. 31148–31158, Dec. 2017.

[43] M. G. Clerc, S. Coulibaly, and M. Tlidi, "Time-delayed nonlocal response inducing traveling temporal localized structures," *Physical Review Research*, vol. 2, p. 013024, Jan. 2020.

[44] S. Yao, C. Bao, P. Wang, and C. Yang, "Generation of stable and breathing flat-top solitons via Raman assisted four wave mixing in microresonators," *Physical Review A*, vol. 101, p. 023833, Feb. 2020.

[45] M. G. Clerc, S. Coulibaly, P. Parra-Rivas, and M. Tlidi, "Nonlocal raman response in kerr resonators: moving temporal localized structures and bifurcation structure," *Chaos*, pp. 2445–2457, Nov. 2002.

[46] L. A. Lugiato and R. Lefever, "Spatial Dissipative Structures in Passive Optical Systems," *Physical Review Letters*, vol. 58, pp. 2209–2211, May 1987.

[47] M. Haelterman, S. Trillo, and S. Wabnitz, "Dissipative modulation instability in a nonlinear dispersive ring cavity," *Optics Communications*, vol. 91, pp. 401–407, Aug. 1992.

[48] Q. Lin and G. P. Agrawal, "Raman response function for silica fibers," *Optics Letters*, vol. 31, pp. 3086–3088, Nov. 2006.

[49] Y. K. Chembo and C. R. Menyuk, "Spatiotemporal Lugiato-Lefever formalism for Kerr-comb generation in whispering-gallery-mode resonators," *Physical Review A*, vol. 87, p. 053852, May 2013.

[50] T. J. Kippenberg, R. Holzwarth, and S. Diddams, "Microresonator-based optical frequency combs," *Science*, vol. 332, no. 6029, pp. 555–559, 2011.

[51] P. Kockaert, P. Tassin, G. Van der Sande, I. Veretennicoff, and M. Tlidi, "Negative diffraction pattern dynamics in nonlinear cavities with left-handed materials," *Physical Review A*, vol. 74, no. 3, p. 033822, 2006.

[52] Z. Ziani, G. Lévêque, A. Akjouj, S. Coulibaly, and A. Taki, "Characterization of spatiotemporal chaos in arrays of nonlinear plasmonic nanoparticles," *Physical Review B*, vol. 100, no. 16, p. 165423, 2019.

[53] U. Peschel, O. Egorov, and F. Lederer, "Discrete cavity solitons," in *Nonlinear Guided Waves and Their Applications*, p. WB6, Optical Society of America, 2004.

[54] J. Cuevas-Maraver, P. G. Kevrekidis, and F. Williams, "The sine-gordon model and its applications," *Nonlinear Systems and Complexity (Switzerland: Springer)*, 2014.

[55] A. Scroggie, W. Firth, G. McDonald, M. Tlidi, R. Lefever, and L. A. Lugiato, "Pattern formation in a passive kerr cavity," *Chaos, Solitons & Fractals*, vol. 4, no. 8-9, pp. 1323–1354, 1994.

[56] D. Gomila and P. Colet, "Transition from hexagons to optical turbulence," *Physical Review A*, vol. 68, p. 011801, July 2003.

[57] D. Gomila and P. Colet, "Fluctuations and correlations in hexagonal optical patterns," *Physical Review E*, vol. 66, p. 046223, Oct. 2002.

[58] N. Prinet, N. Verschueren, and S. Coulibaly, "Eckhaus instability in the Lugiato-Lefever model," *The European Physical Journal D*, vol. 71, p. 243, Sept. 2017.

[59] C. Godey, I. V. Balakireva, A. Coillet, and Y. K. Chembo, "Stability analysis of the spatiotemporal Lugiato-Lefever model for Kerr optical frequency combs in the anomalous and normal dispersion regimes," *Physical Review A*, vol. 89, p. 063814, June 2014.

[60] P. Parra-Rivas, D. Gomila, P. Colet, and L. Gelens, "Interaction of solitons and the formation of bound states in the generalized Lugiato-Lefever equation," *The European Physical Journal D*, vol. 71, p. 198, July 2017.

[61] A. G. Vladimirov, S. V. Gurevich, and M. Tlidi, "Effect of Cherenkov radiation on localized-state interaction," *Physical Review A*, vol. 97, p. 013816, Jan. 2018.

[62] F. Leo, L. Gelens, P. Emplit, M. Haelterman, and S. Coen, "Dynamics of one-dimensional kerr cavity solitons," *Optics express*, vol. 21, no. 7, pp. 9180–9191, 2013.

[63] M. Anderson, F. Leo, S. Coen, M. Erkintalo, and S. G. Murdoch, "Observations of spatiotemporal instabilities of temporal cavity solitons," *Optica*, vol. 3, no. 10, pp. 1071–1074, 2016.

[64] Z. Liu, M. Ouali, S. Coulibaly, M. Clerc, M. Taki, and M. Tlidi, "Characterization of spatiotemporal chaos in a kerr optical frequency comb and in all fiber cavities," *Optics letters*, vol. 42, no. 6, pp. 1063–1066, 2017.

[65] K. Panajotov, M. G. Clerc, and M. Tlidi, "Spatiotemporal chaos and two-dimensional dissipative rogue waves in lugiato-lefever model," *The European Physical Journal D*, vol. 71, no. 7, p. 176, 2017.

[66] K. Panajotov, M. Tlidi, Y. Song, and H. Zhang, "Control of dissipative rogue waves in nonlinear cavity optics: Optical injection and time-delayed feedback," *Chaos: An Interdisciplinary Journal of Nonlinear Science*, vol. 30, no. 5, p. 053103, 2020.

[67] M. Tlidi and K. Panajotov, "Two-dimensional dissipative rogue waves due to time-delayed feedback in cavity nonlinear optics," *Chaos: An Interdisciplinary Journal of Nonlinear Science*, vol. 27, no. 1, p. 013119, 2017.

[68] A. Coillet, J. Dudley, G. Genty, L. Larger, and Y. K. Chembo, "Optical rogue waves in whispering-gallery-mode resonators," *Physical Review A*, vol. 89, p. 013835, Jan. 2014.

[69] G. Agrawal, *Applications of Nonlinear Fiber Optics*. Academic Press, Mar. 2008. Google-Books-ID: HbkKQLPE8yEC.

[70] J. M. Chomaz, "Absolute and convective instabilities in nonlinear systems," *Physical Review Letters*, vol. 69, pp. 1931–1934, Sept. 1992.

[71] P. Coullet, C. Elphick, and D. Repaux, "Nature of spatial chaos," *Physical Review Letters*, vol. 58, pp. 431–434, Feb. 1987.

[72] P. Parra-Rivas, L. Gelens, and F. Leo, "Localized structures in dispersive and doubly resonant optical parametric oscillators," *Physical Review E*, vol. 100, p. 032219, Sept. 2019.

[73] M. G. Clerc, D. Escaff, and V. M. Kenkre, "Analytical studies of fronts, colonies, and patterns: Combination of the Allee effect and nonlocal competition interactions," *Physical Review E*, vol. 82, p. 036210, Sept. 2010.

[74] M. G. Clerc, D. Escaff, and V. M. Kenkre, "Patterns and localized structures in population dynamics," *Physical Review E*, vol. 72, p. 056217, Nov. 2005.

[75] S. M. Allen and J. W. Cahn, "A microscopic theory for antiphase boundary motion and its application to antiphase domain coarsening," *Acta Metallurgica*, vol. 27, pp. 1085–1095, June 1979.

[76] E. Doedel, H. B. Keller, and J. P. Kernevez, "Numerical analysis and control of bifurcation problems (ii): bifurcation in infinite dimensions," *International Journal of Bifurcation and Chaos*, vol. 01, pp. 745–772, Dec. 1991.

[77] E. Doedel, H. B. Keller, and J. P. Kernevez, "Numerical analysis and control of bifurcation problems (i): bifurcation in finite dimensions," *International Journal of Bifurcation and Chaos*, vol. 01, pp. 493–520, Sept. 1991.

[78] J. Knobloch and T. Wagenknecht, "Homoclinic snaking near a heteroclinic cycle in reversible systems," *Physica D: Nonlinear Phenomena*, vol. 206, pp. 82–93, June 2005.

[79] A. Yochelis, J. Burke, and E. Knobloch, "Reciprocal Oscillons and Nonmonotonic Fronts in Forced Nonequilibrium Systems," *Physical Review Letters*, vol. 97, p. 254501, Dec. 2006.

[80] D. Escaff, "Non-local defect interaction in one-dimension: weak versus strong non-locality," *The European Physical Journal D*, vol. 62, pp. 33–38, Mar. 2011.

[81] P. Colet, M. A. Matas, L. Gelens, and D. Gomila, "Formation of localized structures in bistable systems through nonlocal spatial coupling. I. General framework," *Physical Review E*, vol. 89, p. 012914, Jan. 2014.

[82] L. Gelens, M. A. Matas, D. Gomila, T. Dorissen, and P. Colet, "Formation of localized structures in bistable systems through nonlocal spatial coupling. II. The nonlocal Ginzburg-Landau equation," *Physical Review E*, vol. 89, p. 012915, Jan. 2014.

[83] Fernandez-Oto C., Tlidi M., Escaff D., and Clerc M. G., "Strong interaction between plants induces circular barren patches: fairy circles," *Philosophical Transactions of the Royal Society A: Mathematical, Physical and Engineering Sciences*, vol. 372, p. 20140009, Oct. 2014.

[84] D. Escaff, C. Fernandez-Oto, M. G. Clerc, and M. Tlidi, "Localized vegetation patterns, fairy circles, and localized patches in arid landscapes," *Physical Review E*, vol. 91, p. 022924, Feb. 2015.

[85] D. Turaev, M. Radziunas, and A. G. Vladimirov, "Chaotic soliton walk in periodically modulated media," *Physical Review E*, vol. 77, p. 065201, June 2008.

[86] M. Tlidi, A. G. Vladimirov, D. Pieroux, and D. Turaev, "Spontaneous Motion of Cavity Solitons Induced by a Delayed Feedback," *Physical Review Letters*, vol. 103, p. 103904, Sept. 2009.

[87] K. Panajotov, D. Puzyrev, A. G. Vladimirov, S. V. Gurevich, and M. Tlidi, "Impact of time-delayed feedback on spatiotemporal dynamics in the Lugiato-Lefever model," *Physical Review A*, vol. 93, p. 043835, Apr. 2016.

[88] P. Coullet, J. Lega, B. Houchmandzadeh, and J. Lajzerowicz, "Breaking chirality in nonequilibrium systems," *Physical Review Letters*, vol. 65, pp. 1352–1355, Sept. 1990.

[89] D. Gomila, P. Colet, and D. Walgraef, "Theory for the Spatiotemporal Dynamics of Domain Walls close to a Nonequilibrium Ising-Bloch Transition," *Physical Review Letters*, vol. 114, p. 084101, Feb. 2015.

[90] R. Zambrini, M. San Miguel, C. Durniak, and M. Taki, "Convection-induced nonlinear symmetry breaking in

wave mixing," *Physical Review E*, vol. 72, p. 025603, Aug. 2005.

[91] Z. Li, S. Coen, S. G. Murdoch, and M. Erkintalo, "Experimental observations of bright dissipative Kerr cavity solitons and their collapsed snaking in a driven resonator with normal dispersion," *arXiv:2005.02995 [physics]*, May 2020. arXiv: 2005.02995.